CONDENSED MATTER PHYSICS

Microscopic pathways for stress relaxation in repulsive colloidal glasses

F. Dallari[1]*†, A. Martinelli[1†], F. Caporaletti[1], M. Sprung[2], G. Grübel[2], G. Monaco[1†]

Residual stresses are well-known companions of all glassy materials. They affect and, in many cases, even strongly modify important material properties like the mechanical response and the optical transparency. The mechanisms through which stresses affect such properties are, in many cases, still under study, and their full understanding can pave the way to a full exploitation of stress as a primary control parameter. It is, for example, known that stresses promote particle mobility at small length scales, e.g., in colloidal glasses, gels, and metallic glasses, but this connection still remains essentially qualitative. Exploiting a preparation protocol that leads to colloidal glasses with an exceptionally directional built-in stress field, we characterize the stress-induced dynamics and show that it can be visualized as a collection of "flickering," mobile regions with linear sizes of the order of ≈20 particle diameters (≈2 μm here) that move cooperatively, displaying an overall stationary but locally ballistic dynamics.

INTRODUCTION

In the past decades, colloidal glasses have attracted large interest in many scientific and technological sectors (*1*, *2*). Many industrial products are, or happen to be during the production process, colloidal systems (*1*), and many biological materials can be described as complex colloidal glasses or gels (*3*, *4*). The reason of this interest lies in the possibility to easily tune the forces between individual particles allowing control over the material's properties. Depending on the details of the system, this can be achieved, e.g., by adding salts, changing temperature or pressure, and applying electric or magnetic fields (*5*). Stresses left over during the production of these out-of-equilibrium materials can provide another handle to control physical properties (*6*–*8*). One extreme example for network glasses is the historical case of Prince Rupert's drops (*9*). By quenching silicate melt drops in a coolant, Prince Rupert in the seventeenth century produced solid drops with long tails storing large part of the stress field: A drop's head can sustain severe impacts without major consequences, but gently hitting the tail would result in shattering the entire drop. Despite this and other similar effects, the use of stress as a parameter to control the properties of complex systems is still not very common, and more studies are required to fully understand its effects on structural and dynamical properties (*10*).

The microscopic dynamics in disordered matter is typically probed in photon-based scattering experiments (both in the visible and hard x-ray regimes) by measuring the normalized correlation function of the scattered intensity, $g_2(q,t) - 1 = \langle I(0)I(t)\rangle/\langle I\rangle^2 - 1$, where q is the exchanged wave vector, $I(t)$ is the scattered intensity at a given time t, and $\langle\ldots\rangle$ represents the ensemble average (details in the Supplementary Materials). For dilute colloidal solutions, Brownian motion governs density rearrangements, and the $g_2(q,t) - 1$ is characterized by an exponential decay with a relaxation time, τ, proportional to q^{-2} (simple diffusion). Increasing the packing fraction of the solution, the dynamics slows down, the relaxation time grows steeply, and the average relaxation process is described by a Kohlrausch-Williams-Watts (KWW) function $g_2(q,t) - 1 \propto \exp(-2(t/\tau)^{\beta})$ with $\beta \in [0,1]$ (*11*). At a certain volume fraction, the system enters an arrested state, and the relaxation time exceeds any reasonable experimental time scale. If the structure is still amorphous, then we speak of a colloidal glass. However, in many cases, the presence of relatively "fast" dynamics (i.e., movements that take place at accessible laboratory time scales) can still be observed also in otherwise macroscopically arrested systems. The $g_2(q,t) - 1$ in these cases is often described by a KWW function with a "compressed" exponent (i.e., $\beta > 1$) alongside with an anomalous $\tau \propto q^{-1}$ scaling indicating nondiffusive, ballistic dynamics: Examples span from colloidal glasses and gels (*12*), polymers (*13*, *14*), and aerogels (*15*) to metallic glasses (*16*). The wide assortment of materials displaying this characteristic dynamical regime suggests a common underlying mechanism. However, no definitive microscopic description has yet emerged. One model that has proven to be successful is the one initially proposed by Cipelletti *et al.* (*17*) and subsequently by Bouchaud and Pitard (*18*). Simulations based on these ideas report a rich phenomenology compatible with many experimental results (*19*, *20*).

In the present Letter, the characterization of a colloidal glass of repulsive silica nanoparticles in a water-lutidine solution based on x-ray photon correlation spectroscopy (XPCS) experiments is reported (see Materials and Methods for more details). As shown below, the use of samples prepared with an exceptionally directional residual stress field turns out to be the key to provide information on the connection between residual stress and particle dynamics.

RESULTS

Typically, XPCS experiments in small-angle geometry rely on a two-dimensional detector that collects the scattered light in the far-field limit (see the insets of Fig. 1 for typical small angle x-ray scattering patterns): The intensity autocorrelation function at a given q is computed by selecting the appropriate ring-shaped region of interests, and a multispeckle photon correlation analysis is performed (*17*, *21*). As in similar situations, compressed KWW functions are obtained with $\beta = 1.61 \pm 0.14$, as shown in Fig. 1A; it is, however, clear that the long-time behavior of the relaxation function is not correctly described by the KWW expression due to the presence of a stretched tail. This latter feature has been reported for different materials where stress-induced compressed relaxations and nondiffusive dynamics are observed (*14*, *15*, *22*), and its origin has not been clarified yet. In

[1]Dipartimento di Fisica, Università di Trento, I-38123 Povo (Trento), Italy. [2]Deutsches Elektronen-Synchrotron (DESY), Notkestraße 85, 22607 Hamburg, Germany.
*Present address: Deutsches Elektronen-Synchrotron (DESY), Notkestraße 85, 22607 Hamburg, Germany.
†Corresponding author. Email: francesco.dallari@desy.de (F.D.); a.martinelli-2@unitn.it (A.M.); giulio.monaco@unitn.it (G.M.)

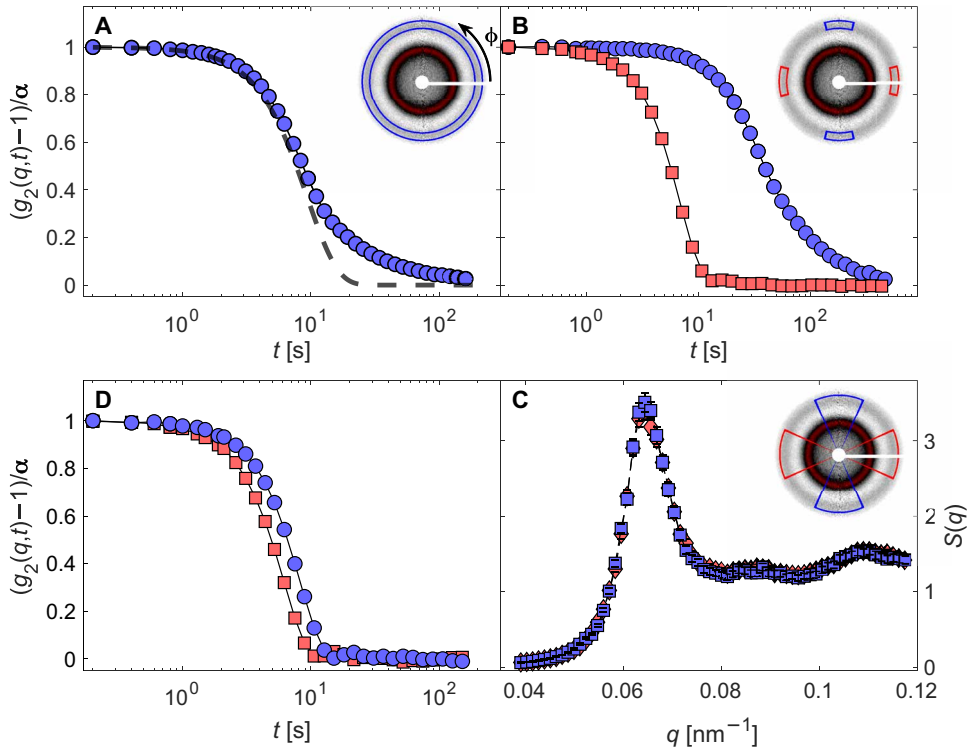

Fig. 1. The dynamics is anisotropic and the structure is not. (**A**) Normalized intensity autocorrelation function, $(g_2(q, t) - 1)/\alpha$ (blue circles) corresponding to $q = (11 \pm 1) \times 10^{-2}$nm^{-1} together with the best-fitting compressed exponential function (dashed line). Here, α is the limit of $g_2(q, t) - 1$ for $t \to 0$. The $g_2(q, t) - 1$ data have been obtained averaging over all pixels within the appropriate ring highlighted in blue for the detector pattern reported in the inset. (**B**) Normalized intensity autocorrelation functions obtained for the same q but selecting different azimuthal angles: Red squares correspond to the horizontal sectors indicated in the inset ($\phi = 0 \pm \pi/12$ and $\phi = \pi \pm \pi/12$), and blue circles correspond to the vertical sectors ($\phi = \pm (\pi/2 \pm \pi/12)$). (**C**) The static structure factor, $S(q)$, corresponding to the same horizontal (red) and vertical (blue) sectors used in (B). No sign of anisotropy in the structure is visible. (**D**) Normalized intensity autocorrelation functions calculated using the horizontal sectors previously discussed and at different ages of the sample: 100 s (red squares) and 400 s (blue circles) after the beginning of the measurement.

the present case, the emergence of this stretched tail can be traced back to the strong anisotropy of the dynamics illustrated in Fig. 1B. Selecting regions out of the same annular ring but for different azimuthal angles ϕ (as defined in the inset of Fig. 1A) leads to different results. It is also possible to get information on static properties looking at the structure factor $S(q) = I(q)/|f(q)|^2$, where $|f(q)|^2$ is the particle form factor (see the Supplementary Materials). No anisotropy is present in $S(q)$, see Fig. 1C. The data obtained using the vertical and horizontal portions of the detector are compatible both in magnitude and peak positions within experimental uncertainties. It has to be outlined that the samples studied here displayed only a mild linear aging behavior (Fig. 1D), with an aging rate $\partial\tau(t_w)/\partial t_w = (0.264 \pm 0.007)$ s/min, where t_w is the time elapsed since the sealing of the capillary (~20 min for this sample). Considering that a single measurement run lasted typically 10 min and that the structure factors measured at the start and at the end of each measurement are identical within experimental uncertainty (see the Supplementary Materials), we can conclude that on the time scale of the experiment, our colloidal glass is stationary.

It is interesting to study the azimuthal angle, ϕ, dependence of the parameters of the KWW function corresponding to the same $|\boldsymbol{q}|$ value. In Fig. 2A, we can see a drastic change in the autocorrelation function in correspondence to the vertical direction that is reflected in a clear drop of the relaxation rate, $(1/\tau)$. More in detail, $1/\tau$ closely follows the absolute value of a cosine function of ϕ (Fig. 2A), meaning that it can be described by a function of the kind: $1/\tau = |\mathbf{q} \cdot \delta\mathbf{v}|$, where $\delta\mathbf{v}$ is a relative velocity field that lies in the horizontal plane. Moreover, the $g_2(q, t) - 1$ functions computed from the horizontal sectors are closely described by the KWW expression with a strongly compressed exponent ($\beta = 2.05 \pm 0.05$ in the example of Fig. 2B), while approaching the vertical direction, the integration over a large distribution of τ values (due to the fact that for $\phi \to \pm \pi/2$, $\tau \to \infty$) produces a stretching of the relaxation function.

Considering only detector sectors in the horizontal plane, where $\cos(\phi) \approx 1$, we can use the KWW as a model to describe the relaxation functions and to investigate the q-dependence of $1/\tau$ and β as reported in Fig. 2 (C and D), respectively. The relaxation rate is proportional to q, clearly indicating a nondiffusive, ballistic dynamics and similarly to what is often found for out-of-equilibrium systems (*12*). The compression exponent has values very close to 2 at all probed q's, indicating a normal distribution for the relative velocity field $\delta\mathbf{v}$. We observe that if sedimentation would be at the basis of the observed dynamics, then the ϕ-dependence of τ would be $\pi/2$-shifted, and therefore, this hypothesis can be ruled out. We also checked by investigating a static sample that vibrations are not playing any role on the time scale of interest here. The reported dynamics here must then correspond to genuine microscopic motions in the horizontal plane.

To characterize in some detail the size of the regions that display such ballistic dynamics, we can evaluate the $\chi_4(q,t)$ function, defined

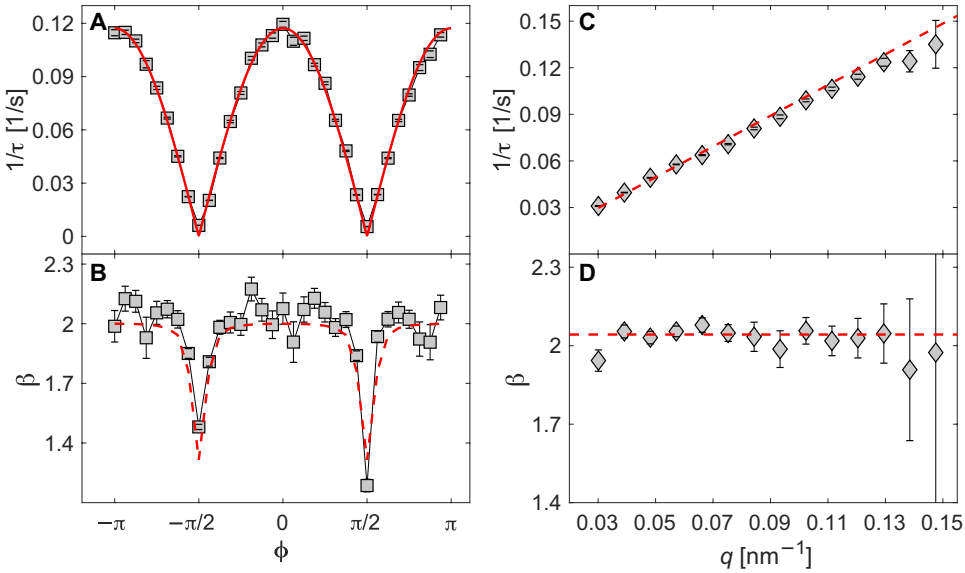

Fig. 2. The dynamics is ballistic and the velocity field lies in the scattering plane. (**A**) Relaxation rates corresponding to $q = (12.0 \pm 0.3) \times 10^{-2}\text{nm}^{-1}$ as a function of the azimuthal angle, ϕ, with 0 corresponding to the horizontal position, see inset of Fig. 1A. The red line corresponds to $|q\delta v \cos(\phi)|$, where $\delta v = (0.97 \pm 0.03)$nm/s is deduced from a fitting procedure. (**B**) Compression exponent, β, of the relaxation function corresponding to the same q value as for (A). The marked decrease in the shape parameter in the vertical direction is an artifact due to the finite ϕ-resolution (here $\delta\phi = \pi/16$), i.e., the vertical sectors see a larger distribution of relaxation times as $\tau \to \infty$ for $\phi \to \pm\pi/2$, and the resulting autocorrelation functions are stretched, as it can be seen from the blue data in Fig. 1B. The red dashed line is obtained from a simple numerical model where a function of the kind $\exp[-2(q\,\delta v\, t \cos(\phi))^2]$is integrated over the experimental q resolution. The average value of β in the horizontal sectors is $\langle\beta(\phi)\rangle_\phi = 2.05 \pm 0.05$. (**C**) Relaxation rate, 1/τ, evaluated for the intensity autocorrelation functions corresponding to the horizontal direction and as a function of q. The red line is a linear fit of $1/\tau = |\mathbf{q}\cdot\delta\mathbf{v}|$, and the obtained value $\delta v = (0.99 \pm 0.02)$nm/s is consistent with that obtained in (A). (**D**) Compression exponent evaluated for the same data as in (C) and as a function of q. The red dashed line is the weighted average, which corresponds to $\beta = 2.04 \pm 0.02$.

as the variance of the normalized intensity correlation function (see the Supplementary Materials). Specifically, we first compute the two-time correlation matrix, defined as $C(t_1, t_2) = \langle I(t_1)I(t_2)\rangle_p / (\langle I(t_1)\rangle_p \langle I(t_2)\rangle_p)$, where $\langle\ldots\rangle_p$ stands for an average over the pixels of the detector. We can observe visible fluctuations of $C(t_1, t_2)$ along the main diagonal (see Fig. 3A), which are a typical sign of heterogeneity in the dynamics (*14*, *23*, *24*). Then, using the method described in (*21*), we can extract clear $\chi_4(q, t)$ signals, see Fig. 3B, peaked at $t^* \approx \tau$.

A more complete study of the dynamical heterogeneities is reported in Fig 4A, where the q and t dependence of the obtained $\chi_4(q,t)$ is shown. At both short ($t \ll \tau$) and long ($t \gg \tau$) time scales, the $\chi_4(q,t)$ has very small values, and a similar behavior is observed as a function of q, with a small $\chi_4(q,t)$ at very large and small q's. The maximum of $\chi_4(q,t)$ is located at the q value corresponding to the $S(q)$ maximum, $q_{\max}$, and at $\tau(q_{\max})$; it is then located at the length scale fixed by the interparticle distance. This result is different from what is observed for a bidimensional version of the studied colloidal glass here (*25*) but is in qualitative agreement with previous experiments on gels (*26*) and with theoretical studies of undercooled liquids (*27*).

It is interesting to point out that the latter results seem to hold here also for glasses characterized by an internal dynamics entirely due to relaxation of mechanical stresses. The most interesting quantity that can be obtained from the $\chi_4(q,t)$ function is its peak value, reported in Fig. 4B as a function of q. This quantity is informative of the number of particles undergoing cooperative motions at the length scale $1/q$ (*28*–*30*), although the presence of a q-dependent prefactor does not allow providing precise estimates (*26*). However, once corrected for the instrumental contrast and multiplied for the number of particles in the scattering volume, we obtain a number of $N_{\text{corr}} \approx 10^4$ cooperatively moving particles at $q = q_{\max}$. This is a very large number, roughly corresponding to regions of ≈2 μm or about 20 particles in linear size. This number is clearly larger than that previously found in confocal microscopy experiments for the clusters of cooperatively rearranging particles in colloidal glasses (*31*). We emphasize here that, as for the $g_2(q,t)$, the $\chi_4(q,t)$ function is strongly ϕ-dependent. Also in this case, the use of a colloidal glass with a strongly directional stress field is the key to extract a reliable value for N_{corr} (see the Supplementary Materials).

DISCUSSION

As recalled earlier, the observation of compressed relaxation functions in colloidal glasses and gels is usually interpreted as an indication of stress relaxation (*12*). This reasonably applies also in the present case: Colloidal glasses have small elastic moduli (*32*), and thus, even moderate forces are sufficient to give rise to strong internal stresses (*33*). This makes very difficult to prepare colloidal glasses with purely isotropic residual stress fields: A somewhat anisotropic dynamics is a quite common leftover after the preparation of colloidal glasses [see, e.g., (*34*)]. What is unexpected here is the almost perfect horizontal alignment of the residual stress field suggested by the fact that all the microscopic rearrangements lie in the horizontal plane. This stress is what remains stored in the sample following its preparation protocol: While stresses in the vertical direction probably have time to relax between the sample preparation phase and the experiment, the stress field in the horizontal plane remains trapped in due to the capillary walls constraints.

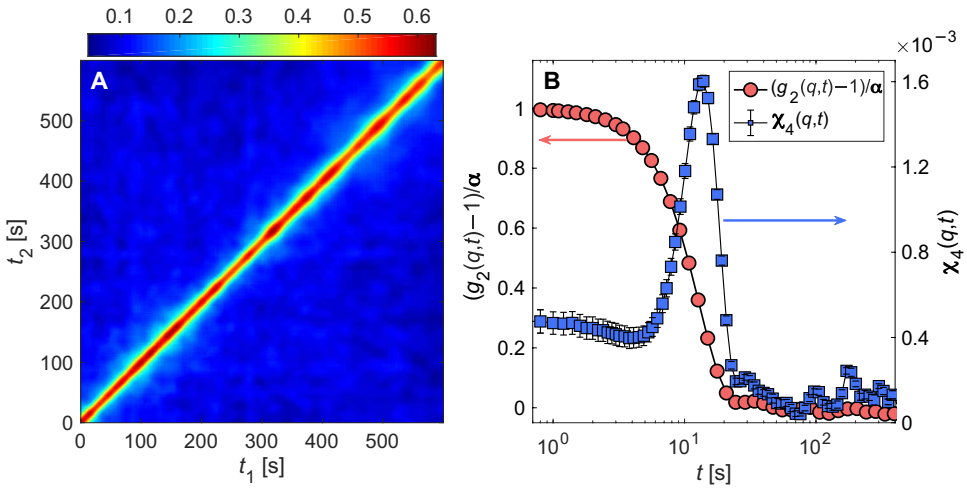

Fig. 3. Evidence of dynamical heterogeneities. (**A**) Two-times autocorrelation matrix computed at the peak, $q_{max} = (6.4 \pm 0.3) \times 10^{-2}$ nm^{-1}, of the structure factor $S(q)$ and obtained selecting only the horizontal sectors within the range $\Delta\phi = \pm \pi/4$. Large fluctuations are clearly visible, being a typical sign of heterogeneous dynamics. (**B**) $\chi_4(q,t)$ (blue squares, right y axis) together with the corresponding normalized intensity autocorrelation function (red circles, left y axis). These data correspond to the same q value as in (A). The $\chi_4(q,t)$ has been computed using the extrapolation scheme described in (*21*).

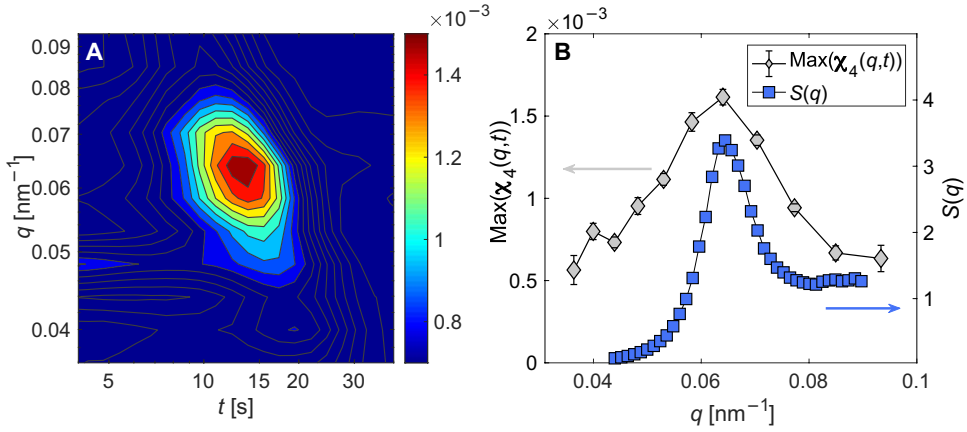

Fig. 4. Wave vector dependence and time dependence of the dynamical heterogeneities. (**A**) Map of the $\chi_4(q,t)$ function. This function is dominated by a single broad peak centered at the q-value corresponding to the interparticle separation and at time $t^* \sim \tau$. (**B**) Comparison between the peak value of the $\chi_4(q,t^*)$ (gray diamonds, left y axis) and the structure factor, $S(q)$ (blue squares, right y axis). Both functions show a maximum at the q value corresponding to the first neighbors distance. Multiplying the maximum of $\chi_4(q,t^*)$ by the total number of particles in the scattering volume [$N = (1.6 \pm 0.3) \times 10^6$ in the present case] and correcting for the instrumental contrast it is possible to obtain an estimate of the number of particles participating in a correlated ballistic motion—a value which is $N_{corr} \approx 10^4$ in the present case.

Whatever is the detailed mechanism leading to this strongly anisotropic stress field, its strong alignment provides us here a tool to correct for it and to extract a clean information on the stress-induced dynamics and, in particular, on the relative velocity field of the particles and on the number of correlated particles in our glass. It is then possible that a certain number of the compressed functions reported in the literature with a stretched tail result from an average of processes over anisotropically stressed regions.

In contrast to the textbook picture of a glass as a frozen liquid, our measurements suggest that it is possible to prepare colloidal glasses, which, at the mesoscopic scale, consist of a collection of mobile regions that rearrange in an intermittent and heterogeneous way with ballistic dynamics following the directions of the residual stresses acting as driving forces. Moreover, the fact that the dynamics is almost stationary suggests that the glass remains trapped in an overall strongly out-of-equilibrium condition, which evolves only very slowly on the time scale of the experiment. In other terms, while the glass is not globally capable of relaxing the stress field stored during the production phase, it is able to relax local stress fields via an intermittent, cooperative dynamics. A similar effect is observed in metallic glasses (*16*) and in numerical simulations (*20*) and might be generic for many different kinds of out-of-equilibrium systems. It remains an interesting problem to understand whether this stress-induced anisotropic mobility discovered in a colloidal glass translates into the possibility of controlling via stress macroscopic transport coefficients as, for example, diffusion.

MATERIALS AND METHODS

Sample preparation

The system studied in this work is a colloidal glass of silica nanoparticles in a nearly critical mixture of water and 2,6-lutidine (*35*).

The nanoparticles were purchased from Micromod under the commercial name of Sicastar. They are plain silica nanoparticles with a nominal diameter of 100 nm, dispersed in pure water with mass concentration of 100 mg per 1 ml of solution, and a polydispersivity index smaller than 0.2. The producer declares a silica nanoparticles density of 2.0 g/cm^3. The lutidine (C_7H_9N), 99% purity, was purchased from Sigma-Aldrich.

To prepare the concentrated colloidal sample, we started from an initial volume ($V_{SiO2} + V_{H2O}$) of the silica-water suspension and then we added lutidine, filtered with a 0.2-μm polytetrafluoroethylene filter, to reach the desired mass concentration (considering the liquid components only) of $C_L^m = 0.25 \pm 0.01$. The obtained suspension was then centrifuged at 15000*g* for 10 min to concentrate all nanoparticles at the bottom of the cuvette. The excess liquid was then removed to reach the desired volume fraction. Subsequently, the nanoparticles were dispersed again in the remaining liquid volume until the sample appeared homogeneous. The colloidal glass was then transferred in thin walled borosilicate capillaries (wall thickness, 0.01 mm; nominal diameter, 0.5 mm). Bubble-free homogeneous samples were obtained by an additional, mild centrifugation at 100*g* for 60 s, and they were eventually flame-sealed in the capillaries. The obtained volume fraction was measured by x-ray transmission; this procedure allowed us also to check the sample's homogeneity (see the Supplementary Materials).

Colloidal suspensions of silica nanoparticles dispersed in water-lutidine mixture are known to have the ability to change the interparticle interaction switching from a repulsive potential to an attractive one in a narrow temperature interval inducing an aggregation in dilute systems (*36*) or a glass-glass transition in concentrated ones as observed in (*37*). All the measurements reported here were carried out at a fixed temperature of 298.15 K, i.e., well below the onset of the wetting regime and within the repulsive glass region (*35*, *37*).

XPCS experiment

The XPCS experiment in small-angle geometry was performed at the coherent x-ray scattering beamline P10 (*38*) of the Petra III storage ring in Hamburg (D). The x-ray beam energy of 8 keV with a bandwidth $\Delta E \approx 1$ eV was selected using a Si(111) monochromator. The beam was focused at the sample position to a spot of 2 μm × 3 μm full width at half maximum ($V \times H$). The speckle patterns were acquired using an Eiger 4M area detector (pixel size, 75 μm × 75 μm; 2167 pixels × 2070 pixels) positioned in forward scattering at a distance of 5 m downstream of the sample. The typical integration time per frame ranged from 0.1 to 1 s for a total of few thousands images per measurement.

The sample was mounted in a vacuum chamber directly connected to the upstream optics vacuum chambers and to the downstream fly path reaching out the detector position. The detector itself was in air, separated from the fly path by a Kapton window. Before the start of the measurements, a careful characterization of sample damage under x-ray illumination was performed. We found that up to a total absorbed dose of 30 MGy, no beam damage effects were detected. The data reported here correspond to a maximum total absorbed dose of 15 MGy [over the whole series of images acquired to obtain one $g_2(q,t)$ signal]. This was achieved using attenuators to reduce the beam flux to a value of $\approx 1.5 \times 10^8$ ph/s.

The results reported here were reproduced on several samples prepared following the same protocol described above in two different beamtimes at beamline P10 at Petra. Two samples with different polydispersity were also investigated, and qualitatively, similar results were obtained (*39*). We are then confident that polydispersity is not playing a critical role here. For clarity, only some representative results are here presented.

SUPPLEMENTARY MATERIALS

Supplementary material for this article is available at http://advances.sciencemag.org/cgi/content/full/6/12/eaaz2982/DC1

REFERENCES AND NOTES

1. T. Cosgrove, *Colloid Science: Principles, Methods and Applications* (Wiley-Blackwell, ed. 2, 2010).
2. P. D. Howes, R. Chandrawati, M. M. Stevens, Colloidal nanoparticles as advanced biological sensors. *Science* **346**, 1247390 (2014).
3. O. Lieleg, J. Kayser, G. Brambilla, L. Cipelletti, A. R. Bausch, Slow dynamics and internal stress relaxation in bundled cytoskeletal networks. *Nat. Mater.* **10**, 236–242 (2011).
4. T. E. Angelini, E. Hannezo, X. Trepat, M. Marquez, J. J. Fredberg, D. A. Weitz, Glass-like dynamics of collective cell migration. *Proc. Natl. Acad. Sci. U.S.A.* **108**, 4714–4719 (2011).
5. J. Israelachvili, *Intermolecular and Surface Forces* (Academic Press, ed. 3, 2011), pp. 291–340.
6. D. J. Green, R. Tandon, V. M. Sglavo, Crack arrest and multiple cracking in glass through the use of designed residual stress profiles. *Science* **283**, 1295–1297 (1999).
7. Y. Zhang, W. H. Wang, A. L. Greer, Making metallic glasses plastic by control of residual stress. *Nat. Mater.* **5**, 857–860 (2006).
8. R. E. Fischer, B. Tadic-Galeb, P. R. Yoder, *Optical System Design* (Mc Graw Hill, ed. 2, 2000).
9. L. Brodsley, F. C. Frank, J. W. Steeds, Prince Rupert's drops. *Notes Rec. R. Soc. Lond.* **41**, 1–26 (1986).
10. M. Ballauff, J. M. Brader, S. U. Egelhaaf, M. Fuchs, J. Horbach, N. Koumakis, M. Krüger, M. Laurati, K. J. Mutch, G. Petekidis, M. Siebenbürger, T. Voigtmann, J. Zausch, Residual stresses in glasses. *Phys. Rev. Lett.* **110**, 215701 (2013).
11. G. Williams, D. C. Watts, Non-symmetrical dielectric relaxation behaviour arising from a simple empirical decay function. *Trans. Faraday Soc.* **66**, 80–85 (1970).
12. L. Cipelletti, L. Ramos, Slow dynamics in glassy soft matter. *J. Phys. Condens. Matter* **17**, 253–285 (2005).
13. H. Guo, G. Bourret, M. K. Corbierre, S. Rucareanu, R. B. Lennox, K. Laaziri, L. Piche, M. Sutton, J. L. Harden, R. L. Leheny, Nanoparticle motion within glassy polymer melts. *Phys. Rev. Lett.* **102**, 075702 (2009).
14. H. Conrad, F. Lehmkühler, B. Fischer, F. Westermeier, M. A. Schroer, Y. Chushkin, C. Gutt, M. Sprung, G. Grübel, Correlated heterogeneous dynamics in glass-forming polymers. *Phys. Rev. E* **91**, 042309 (2015).
15. A. Madsen, R. L. Leheny, H. Guo, M. Sprung, O. Czakkel, Beyond simple exponential correlation functions and equilibrium dynamics in x-ray photon correlation spectroscopy. *New J. Phys.* **12**, 055001 (2010).
16. B. Ruta, Y. Chushkin, G. Monaco, L. Cipelletti, E. Pineda, P. Bruna, V. M. Giordano, M. Gonzalez-Silveira, Atomic-scale relaxation dynamics and aging in a metallic glass probed by x-ray photon correlation spectroscopy. *Phys. Rev. Lett.* **109**, 165701 (2012).
17. L. Cipelletti, S. Manley, R. C. Ball, D. A. Weitz, Universal aging features in the restructuring of fractal colloidal gels. *Phys. Rev. Lett.* **84**, 2275–2278 (2000).
18. J.-P. Bouchaud, E. Pitard, Anomalous dynamical light scattering in soft glassy gels. *Eur. Phys. J. E* **9**, 287–291 (2002).
19. M. Bouzid, J. Colombo, L. V. Barbosa, E. Del Gado, Elastically driven intermittent microscopic dynamics in soft solids. *Nat. Commun.* **8**, 15846 (2017).
20. N. Gnan, E. Zaccarelli, The microscopic role of deformation in the dynamics of soft colloids. *Nat. Phys.* **15**, 683–688 (2019).

21. A. Duri, H. Bissig, V. Trappe, L. Cipelletti, Time-resolved-correlation measurements of temporally heterogeneous dynamics. *Phys. Rev. E* **72**, 051401 (2005).
22. H. Guo, J. N. Wilking, D. Liang, T. G. Mason, J. L. Harden, R. L. Leheny, Slow, nondiffusive dynamics in concentrated nanoemulsions. *Phys. Rev. E* **75**, 041401 (2007).
23. L. Berthier, G. Biroli, Theoretical perspective on the glass transition and amorphous materials. *Rev. Mod. Phys.* **83**, 587–645 (2011).
24. P. Ballesta, A. Duri, L. Cipelletti, Unexpected drop of dynamical heterogeneities in colloidal suspensions approaching the jamming transition. *Nat. Phys.* **4**, 550–554 (2008).
25. Z. Zhang, P. J. Yunker, P. Habdas, A. G. Yodh, Cooperative rearrangement regions and dynamical heterogeneities in colloidal glasses with attractive versus repulsive interactions. *Phys. Rev. Lett.* **107**, 208303 (2011).
26. V. Trappe, E. Pitard, L. Ramos, A. Robert, H. Bissig, L. Cipelletti, Investigation of q-dependent dynamical heterogeneity in a colloidal gel by x-ray photon correlation spectroscopy. *Phys. Rev. E* **76**, 051404 (2007).
27. P. Charbonneau, D. R. Reichman, Dynamical heterogeneity and nonlinear susceptibility in supercooled liquids with short-range attraction. *Phys. Rev. Lett.* **99**, 135701 (2007).
28. L. Berthier, G. Biroli, J.-P. Bouchaud, L. Cipelletti, D. El Masri, D. L'Hôte, F. Ladieu, M. Pierno, Direct experimental evidence of a growing length scale accompanying the glass transition. *Science* **310**, 1797–1800 (2005).
29. L. Berthier, G. Biroli, J.-P. Bouchaud, R. L. Jack, Overview of different characterizations of dynamic heterogeneity, in *Dynamical Heterogeneities in Glasses, Colloids, and Granular Media* (Oxford Univ. Press, 2011).
30. W. K. Kegel, A. von Blaaderen, Direct observation of dynamical heterogeneities in colloidal hard-sphere suspensions. *Science* **287**, 290–293 (2000).
31. E. R. Weeks, J. C. Crocker, A. C. Levitt, A. Schofield, D. A. Weitz, Three-dimensional direct imaging of structural relaxation near the colloidal glass transition. *Science* **287**, 627–631 (2000).
32. R. Kesavamoorthy, A. K. Arora, Elastic constants of colloidal glass. *J. Phys. C* **19**, 2833 (1986).
33. M. Fuchs, M. E. Cates, Theory of nonlinear rheology and yielding of dense colloidal suspensions. *Phys. Rev. Lett.* **89**, 248304 (2002).
34. L. Cipelletti, L. Ramos, S. Manley, E. Pitard, D. A. Weitz, E. E. Pashkovski, M. Johansson, Universal non-diffusive slow dynamics in aging soft matter. *Faraday Discuss.* **123**, 237–251 (2003).
35. D. Beysens, D. Estève, Adsorption phenomena at the surface of silica spheres in a binary liquid mixture. *Phys. Rev. Lett.* **54**, 2123–2126 (1985).
36. D. Pontoni, T. Narayanan, J.-M. Petit, G. Grübel, D. Beysens, Microstructure and dynamics near an attractive colloidal glass transition. *Phys. Rev. Lett.* **90**, 188301 (2003).
37. X. Lu, S. G. J. Mochrie, S. Narayanan, A. R. Sandy, M. Sprung, How a liquid becomes a glass both on cooling and on heating. *Phys. Rev. Lett.* **100**, 045701 (2008).
38. P10 Coherence Applications Beamline; http://photon-science.desy.de/facilities/petra_iii/beamlines/p10_coherence_applications/index_eng.html.
39. F. Dallari, Thesis, University of Trento (2018).
40. B. J. Berne, R. Pecora, *Dynamic Light Scattering. With Applications to Chemistry, Biology, and Physics* (Wiley-Interscience, 1976).
41. G. Grübel, A. Madsen, A. Robert, X-Ray Photon Correlation Spectroscopy (XPCS), in *Soft Matter Characterization*, R. Borsali, R. Pecora, Eds., (Springer Netherlands, 2008), pp. 953–995.
42. The Center For X-ray Optics, www.cxro.lbl.gov/.
43. S. R. Aragón, R. Pecora, Theory of dynamic light scattering from polydisperse systems. *J. Chem. Phys.* **64**, 2395–2404 (1976).
44. A. Fluerasu, P. Kwasniewski, C. Caronna, F. Destremaut, J.-B. Salmon, A. Madsen, Dynamics and rheology under continuous shear flow studied by x-ray photon correlation spectroscopy. *New J. Phys.* **12**, 035023 (2010).
45. S. Busch, T. H. Jensen, Y. Chushkin, A. Fluerasu, Dynamics in shear flow studied by X-ray Photon Correlation Spectroscopy. *Eur. Phys. J. E* **26**, 55–62 (2008).
46. J. Möller, T. Narayanan, Velocity fluctuations in sedimenting brownian particles. *Phys. Rev. Lett.* **188**, 198001 (2017).
47. L. Berthier, Dynamic heterogeneity in amorphous materials. *Phys. Ther.* **4**, 42 (2011).
48. C. Toninelli, M. Wyart, L. Berthier, G. Biroli, J.-P. Bouchaud, Dynamical susceptibility of glass formers: Contrasting the predictions of theoretical scenarios. *Phys. Rev. E* **71**, 041505 (2005).

Acknowledgments: We acknowledge DESY (Hamburg, Germany), a member of the Helmholtz Association HGF, for the provision of experimental facilities. Parts of this research were carried out at Petra III, beamline P10 (experiment numbers: I-20170461 EC and I-20180249 EC). **Funding:** The research leading to this result has been supported by the project CALIPSOplus under the Grant Agreement 730872 from the EU Framework Programme for Research and Innovation HORIZON 2020. **Author contributions:** F.D., A.M., and G.M conceived and designed the research. F.D. and A.M. prepared and characterized the samples. F.D. and A.M performed the data analysis, with inputs from G.M. F.D., A.M., F.C., M.S., G.G., and G.M. performed the experiment. F.D., A.M., and G.M wrote the paper, with contributions from all the authors. **Competing interests:** The authors declare that they have no competing interests. **Data and materials availability:** All data needed to evaluate the conclusions in the paper are present in the paper and/or the Supplementary Materials. Additional data related to this paper may be requested from the authors.

Submitted 28 August 2019
Accepted 12 December 2019
Published 20 March 2020
10.1126/sciadv.aaz2982

Citation: F. Dallari, A. Martinelli, F. Caporaletti, M. Sprung, G. Grübel, G. Monaco, Microscopic pathways for stress relaxation in repulsive colloidal glasses. *Sci. Adv.* **6**, eaaz2982 (2020).

Science Advances

Microscopic pathways for stress relaxation in repulsive colloidal glasses

F. Dallari, A. Martinelli, F. Caporaletti, M. Sprung, G. Grübel and G. Monaco

Sci Adv **6** (12), eaaz2982.
DOI: 10.1126/sciadv.aaz2982

Science Advances (ISSN 2375-2548) is published by the American Association for the Advancement of Science, 1200 New York Avenue NW, Washington, DC 20005. The title *Science Advances* is a registered trademark of AAAS.